Materials Transactions, Vol. 62, No. 11 (2021) pp. 1604 to 1608

Superior Strength and Ultrahigh Ductility in Hierarchical Structured 2205 Duplex Stainless Steel from Nanoscale to Microscale

Jie Sheng[1,2,3], Jing Jin[1], Yu Shi[1], Weiqian Chen[1,2], Guocai Ma[1,3], Jiafu Wei[1], Yuehong Zheng[1], Xin Guo[1], Faqi Zhan[1], Peiqing La[1,*] and Raab Georgiy I.[4]

[1]*State Key Laboratory of Gansu Advanced Non-Ferrous Metal Materials, Lanzhou University of Technology, Lanzhou 730050, China*
[2]*Gansu Key Laboratory of Solar Power System Engineering Project, Jiuquan Vocational and Technical College, Jiuquan 735100, China*
[3]*Jiuquan Iron and Steel Group, Jiayuguan 735000, China*
[4]*Ufa State Aviation Technical University, 12 K. Marx str., Ufa 450008, Russia*

A laminated structured 2205 duplex stainless steel (DSS) with graded grain size was prepared via aluminothermic reaction and subsequent hot rolling with deformation of 80% at 1000°C, and its mechanical properties, strengthening and toughening mechanism were studied. Our materials have extraordinary elongation of 54% and high tensile strength of 990 MPa. The lamellar structure is characterized with heterogeneous lamella austenite (with nano-grain, ultrafine grain, micro-grain and nano-twin) and ferrite (with ultrafine grain and a proper amount of micro grain) coalesced alternately. The high strength is attributed to strengthening of complex grain (distribution from nanoscale to microscale) and interfaces arising from hierarchical and laminated dual-phase heterogeneous structure and distribution. The unusual high ductility is thought to be mainly attributed to the lamellar structure and dislocation hardening. [doi:10.2320/matertrans.MT-M2021085]

(Received May 25, 2021; Accepted August 4, 2021; Published October 25, 2021)

Keywords: *2205 DSS, laminated structured, microstructure, plastic deformation mechanisms, strength-ductility balance*

1. Introduction

With the improvement of level of strength of materials, plastic problem has become the bottleneck of high performance processing for material.[1)] How to enhance the plasticity of the high strength reinforced plastic.[2)] It is well known that metals and alloys can be strengthened when their grains sizes were reduced to nanoscale, but which leads to deterioration of ductility and brittleness.[3)] Nanoscale materials do not avoid the strength-ductility trade-off which has been a dilemma for centuries in materials science and engineering.[4)]

To break the dilemma, inhomogeneous geometry, spatial distribution, multi-scale grain size, multi-phase, non-uniform composition distribution and lamella structured metal materials have been used to optimizing their mechanical properties.[5)] Researches were inspired by natural world materials, such as bamboo, tooth and bone which are graded materials.[6)] Graded materials that are characterized by the composition, microstructure and properties varying with a spatial gradient, are not uncommon in impressive natural material systems due to nature selection for performance optimization. In fact, materials design has long been utilized in nature by optimizing the mechanical properties of numerous biological, for example, biological bones have good strength and toughness.[7)] Inspired by the excellent fracture toughness of bones, Koyama *et al.* verified the superior fatigue crack resistance in metastable multiphase steels with an intrinsic lamellae consisting of lamellar martensite and a metastable austenite phase that is comparable to bone structure.[8,9)] In recent years, material scientists have developed metallic materials with nano-gradient structure,[10,11)] heterogeneous structure[12)] and "bi-modal" structure,[13)] enabling them to simultaneously obtain high strength and high plasticity. In general, there is no developed method to simultaneously improve the strength and ductility a lot in comparison to the conventional one.

Inspired by excellent combination of strength and plasticity of bone, in this work, a hierarchical structured 2205 duplex stainless steel (DSS) was designed and prepared via aluminothermic reaction and followed by rolled at 1000°C with 80% thickness reduction, which exhibits superior strength and ultrahigh ductility in alloys.

2. Materials and Methods

The chemical composition of the cast ingot 2205 DSS was 0.01C–0.93Mn–0.28Si_3N_4–17.7Cr–3.41Ni–1.98Mo–20.15Al–67Fe_2O_3 in weight percent, which was prepared via aluminothermic reaction. Aluminothermic reaction was a method to obtain high melting point metal by using the reducibility of aluminum. The experiment was depended on thermite reaction equation $3Fe_2O_3 + 8Al \rightarrow 2Fe_3Al + 3Al_2O_3$. Details information on the processing was reported elsewhere.[14,15)]

The ingot was cut as strip samples and placed in a resistance heating furnace heated to 1000°C for 10 minutes. The rolling thickness reduction was 80% and the corresponding samples was thinned from 5 mm to 1 mm with keeping for 5 minutes at 1000°C after each rolled. Finally, the rolled specimen is air cooled to room temperature.

The microstructures were characterized by A JSM-6700F scanning electron microscope (SEM) in the secondary mode and Zeiss Ultra 55 electron back-scatter diffraction (EBSD). A JEM-2010 transmission electron microscope (TEM) operated at 200 kV was used for TEM observations. Thin foils for TEM observations were mechanically grind to a thickness of 50 μm followed by electrochemical thinning using a twin-jet electro-polishing device in a solution of 5 vol% perchloric acid in ethanol. Dog-bone shaped tensile samples were machined by a wire electrical discharge

*Corresponding author, E-mail: pqla@lut.cn

milling, the cutting direction parallel to the rolling direction.[16,17] And the tensile samples have a gauge length of 32 mm and cross-section of $3.2 \times 0.5\,mm^2$. Uniaxial tensile tests were carried out at room temperature using a AT10t universal mechanical testing machine with a maximum loading capacity of 100 kN operating at a crossing speed of 0.2 mm/min.

3. Results

3.1 Microstructure of the hierarchical structured 2205 DSS

The initial microstructure of the as-cast 2205DSS is presented in Fig. 1(a), and the microstructure is composed of ferrite and austenite. After hot rolled, the austenite and ferrite grains would be elongated into a lamellar structure with slightly curved morphology along rolling direction (RD), which is indicated by a white arrow (Fig. 1(b)).

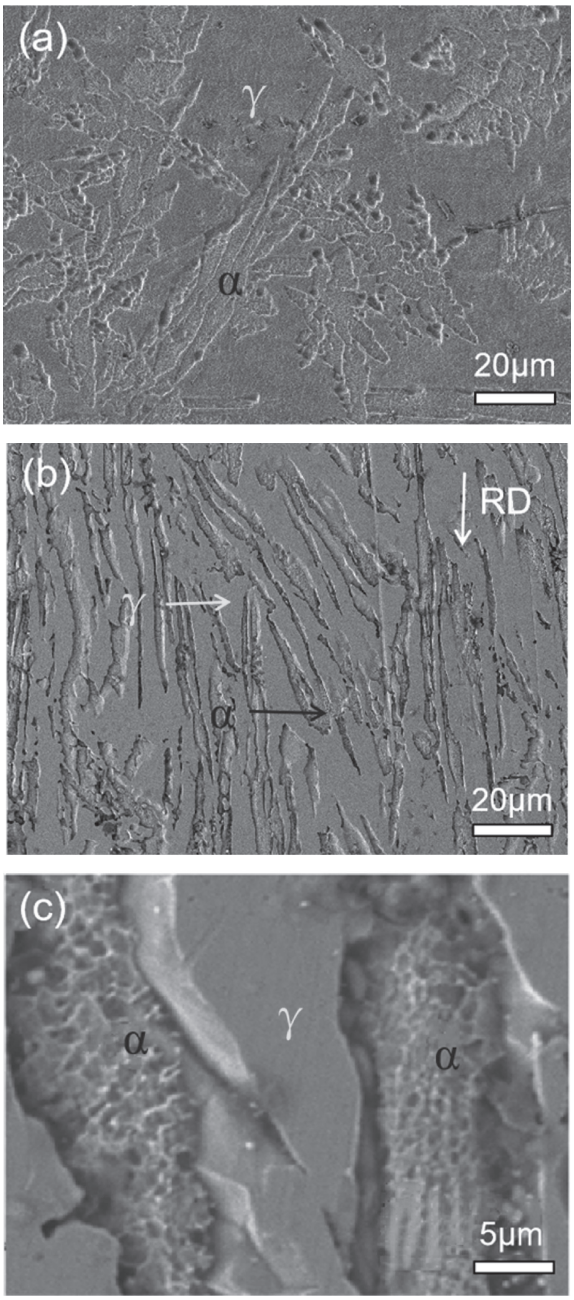

Fig. 1 SEM micrographs of the 2205 DSS before and after hot rolling: (a) initial microstructure of the steel, (b) low and (c) high power microstructure of the hot rolled steel.

In the image quality (IQ) phase maps (Fig. 2(a)), the blue- and red-colored grains are correspond to γ and α. It can be seen that the 2205 DSS possesses a heterogeneous phase structure in which austenite are embedded in a ferrite matrix. The 2205 DSS specimen exhibited a dual-phase microstructure with a laminated morphology (Fig. 2(a)), as shown in the SEM micrograph (Fig. 1(b)). These γ grains exhibited a relatively inhomogeneous orientation distribution, α grains occupied a large area with the same orientation (Fig. 2(b)). The volume fraction of austenite is about 45%, and the ferrite fraction is about 55% (Fig. 2(a)). Some austenite grains have twin boundaries and the majority of grains have substructures as shown in high-magnification EBSD grain boundaries map (Fig. 2(c)). Average aspect ratio of the grains was also estimated and the value is 2.65. Statistical distribution histogram of grain size obtained from Fig. 2(c) is exemplified in Fig. 2(d), which shows that gains less than 400 nm is about 45%.

The ferrite lamellae phase mainly consists of ultrafine grains (Fig. 1(c)) and a proper amount of micro grains (Fig. 2(a)), austenite phase also has a heterogeneous microstructure, including micron grains, ultrafine grains (Fig. 2(a)), nano grains (Fig. 3(a), and 3(b)) and nano-twins (Fig. 3(c), (d)). The small and big black spots in bright field (BF)-TEM (Fig. 3(a)) are nanocrystalline and sub-microcrystalline, respectively. And corresponding SAED inserted identifies austenite crystal in ring patterns. The bright fine spots in dark field (DF)-TEM (Fig. 3(b)) exhibits austenite nanocrystalline. In Fig. 3(c), the BF-TEM image and SAED pattern confirm the formation of mechanical twins, and show dislocation forest along the twin boundaries. It also can be founded that twin boundaries and dislocation forest interaction made twin boundaries imperfect. Further, the DF-TEM images shown in Fig. 3(d). The twin bundles can be clearly observed, consisting of several parallel, straight, thin twins. The average twin boundary spacing is about 18 nm.

3.2 Mechanical properties and strain hardening of the hierarchical 2205 DSS

Tensile properties of the hierarchical 2205 DSS on room temperature are presented in Fig. 4. To emphasize the substantial improvement in mechanical property, the uniaxial tensile engineering stress-strain curves of the present hierarchical and conventional 2205 DSS are presented for comparison in Fig. 4(a). The hierarchical 2205 DSS shows an extraordinary combination of high yield strength and ultrahigh uniform ductility. The yield strength reaches as high as 780 MPa, and the ultimate tensile strength up to 990 MPa. More intriguingly, the hierarchical 2205 DSS also shows a large tensile ductility, with a uniform elongation of 54%. The elongation is the highest in the reported duplex stainless steels with high ultimate tensile strength level of 1 GPa. The hierarchical 2205 DSS has much higher strain hardening rate ($\Theta = d\sigma/d\varepsilon$), especially at large strain (Fig. 4(b)). The work-hardening rate curve reveals a multi-stage work-hardening response, Θ shows a upturn at first and then drops, which has never been observed in traditional homogeneous steels,

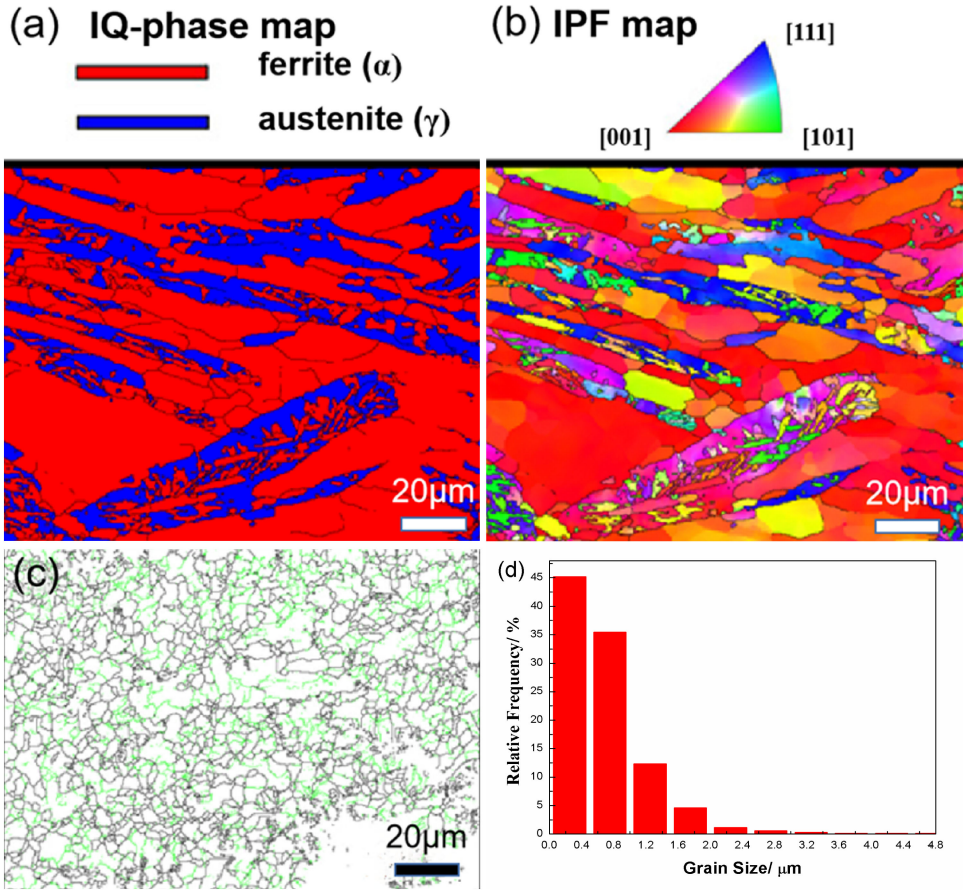

Fig. 2 EBSD (a) IQ-phase maps and (b) inverse pole figure (IPF) maps of the 2205 DSS. In the phase map austenite (γ) and ferrite (α) are indexed as blue and red; (c) Grain boundaries map, green line represents low-angle grain boundaries ($2° < \text{misorientation angle} \leq 10°$) and black line represents high-angle grain boundaries (misorientation angle $> 10°$); (d) Grain size distribution of the steel.

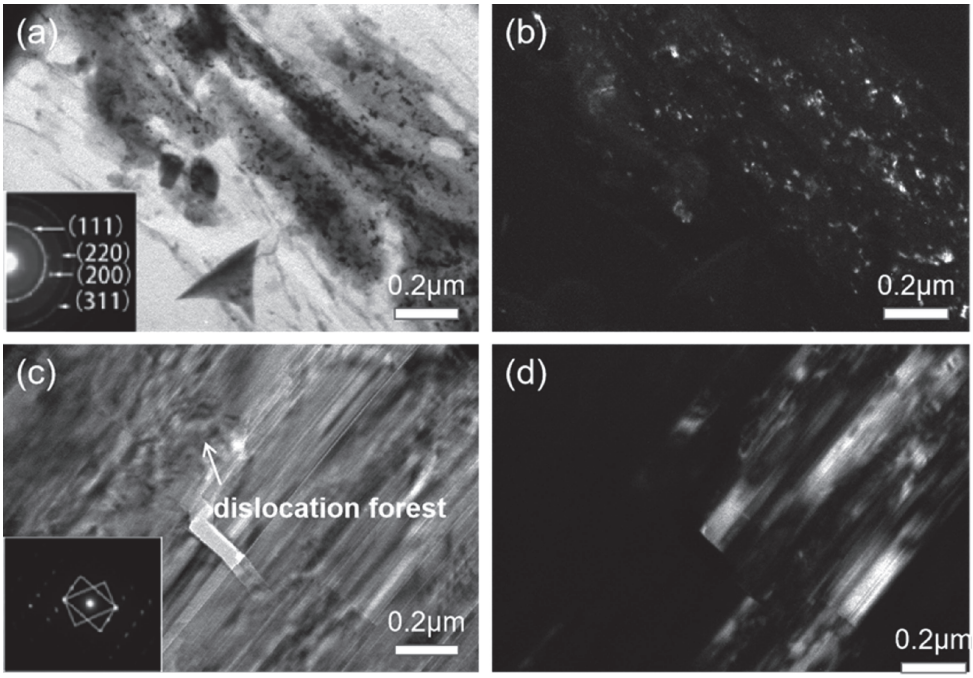

Fig. 3 (a) BF-TEM image and selected area electron diffraction pattern (SAED) image inserted down left; (b) DF-TEM image; (c), (d) a high density nanotwins large TEM image in austenite phase (up inset, SAED).

indicating a discontinuous yielding. High Θ of the 2205 specimen is responsible for its ultrahigh ductility. Figure 4(c) shows the plots of ultimate tensile strength versus elongation to fracture. Evidently, strength$*$elongation of the present hierarchical steel super above strength$*$elongation line, shows an unprecedented synergy of both ultrahigh strength

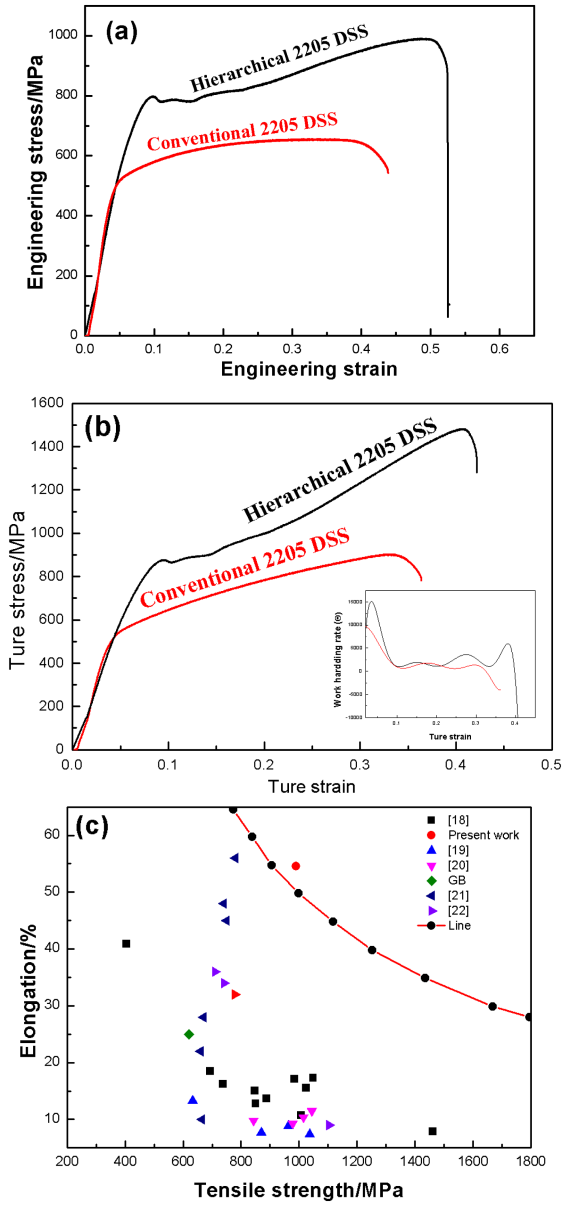

Fig. 4 The hierarchical 2205 stainless steel and conventional 2205 stainless steel: (a) tensile engineering stress-strain curves; (b) representative true stress-strain curves form (a). Inset exhibits the strain-hardening rate (Θ)-true strain curves; (c) strength-elongation plot of selected duplex stainless steels.

and large uniform ductility compared with other duplex stainless steels.

The samples for tensile testing have a rectangular cross-section of $2 \times 1\,mm^2$ and a gauge length of 8 mm.[18] Cylindrical tensile test specimens with a diameter of 4 mm and a gage length of 20 mm were machined. Tensile specimens with a gage length of 25.4 mm were machined. Tensile specimens with a thickness of 1.2 mm, length of 10 mm, and width of 2.2 mm.

3.3 Fracture morphology of the hierarchical 2205 DSS

Fractography was presented using the SEM, as shown in Fig. 5. Fracture surface at low magnification appears to be light and dark gray areas, while do not appear bright or granular which due to reflection of light from the flat cleavage surfaces. Interestingly, the striations (dark gray

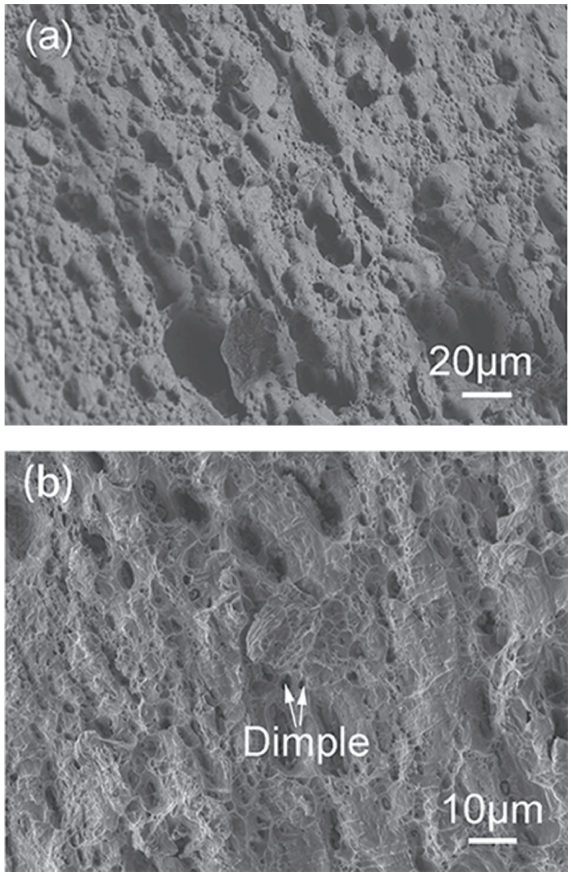

Fig. 5 The SEM fractographs of the hierarchical 2205 DSS.

areas) that are nearly parallel to one another are observed (Fig. 5(a)). This indicates that the fracture was accompanied by severe plastic deformation prior to failure. When the fracture surface is magnified, a great number of fine dimples and fibrous which is caused by shear were observed in Fig. 5(b). Micro-voids nucleate and grow, and eventually tear between the micro voids fracture. This type of fracture surface denotes a typical ductile fracture, which consists with the ultrahigh ductility of the hierarchical 2205 DSS.

4. Discussions

Eight approaches were summarized by E. Ma to improve the ductility of nanocrystalline materials.[19] These approaches were mainly realized by promoting strain hardening and accelerating strain hardening rate. Bimodal and multi-modal grain size nanocrystalline materials were prepared by mixing up the length scales, specifically by creating a bimodal (or multi-modal) grain size distribution, one could achieve simultaneously good yield strength and fairly large uniform elongation. When bimodal structure was created on the nano-micro-scale, a large gain in work hardening and uniform strain was achieved, with only a small loss of strength.

The hierarchical 2205 DSS with twisted lamellar mixture of ferrite and austenite phases shows the micro/sub-microcrystalline ferrite phase but micro/nanocrystalline and nanotwin austenite phase, quite similar to the microstructure of bone. Strength coexists with toughness by virtue of bone's twisted hierarchical and heterogeneous mixture (soft and

hard) substructure which simultaneous activate of multiple micro mechanisms to exceptional improvements stiffness and toughness.[20] We hypothesized that a similar mechanical response can be transferred to steels by processing a similar multiphase heterogeneous hierarchical microstructure to benefit from the discontinuous yielding and interface structure and distribute effect.

The heterogeneous lamella dual-phase microstructure can be considered as a derivative of bimodal structure, but is much more effective in producing work hardening than the reported conventional bimodal structure.[21,22] Compared with the conventional bimodal structure, the heterogeneous lamella dual-phase microstructure possesses the following unique features that are essential for producing the high strength coexists with high ductility: (i) the graded hierarchical nature of the structure, (ii) the duplex mixture and multiscale grains, and (iii) the complex of interlamella interfaces. First, it has been reported that the elongated inclusions produce higher strain hardening than spherical ones, especially when its long axis is aligned in the loading direction, which is the case in this work. The graded hierarchical morphology enables the hard and soft modes of dislocation glide behaviour. In the hard mode, dislocations glide on the slip systems inclined to the lamellar direction and are thus constrained by the small lamellar spacing. In the soft mode, dislocations travel parallel to the lamellar direction and thus experience less resistances from twin or elongated grain boundaries.[23] Second, the duplex mixture and multiscale grains can induce multiple plastic strain gradients under uniaxial loading conditions to develop complex back stresses than the conventional bimodal structure. Third, the heterogeneous lamella dual-phase microstructure has complex and the high density of interlamella interfaces, where dislocation can pile up and accumulate to enhance backstress hardening and dislocation hardening. Therefore, high back stress and dislocation hardening are responsible for the high strength and ductility.

5. Conclusions

(1) A hierarchical duplex structure with heterogeneous grains from nanoscale to microscale was created in 2205 DSS. The elongation of 54% and high tensile strength of 990 MPa.

(2) In essence, the graded hierarchical geometry and dual-phase with multiscale grain size distribution simultaneous activate of multiple plastic deformation mechanisms, enabling the steel effective for developing back stress and dislocations hardening which are mainly responsible for the observed superior strength and ultrahigh ductility.

Acknowledgments

This work was supported by the National Natural Science Foundation of China [Grant No. 51911530119]; Natural Science Foundation of Gansu Province [Grant No. 21JR5RA450]; Project supported by the Department of Education of Gansu Province Innovation Fund [Grant No. 2021A-023]; and Open Project Fund of Gansu Key Laboratory of Solar Power System Engineering Project [Grant No. 2021SPEK01].

REFERENCES

1) X.Y. Zhang, D. Jiao, S.X. Li, C.Y. Li and Z.Z. Yuan: Mater. Trans. **60** (2019) 969–974.
2) Y.J. Wei, Y.Q. Li, L.C. Zhu, Y. Liu, X.Q. Lei, G. Wang, Y.X. Wu, Z.L. Mi, J.B. Liu, H.T. Wang and H.J. Gao: Nat. Commun. **5** (2014) 3580.
3) E. Ma: Scr. Mater. **49** (2003) 663–668.
4) C.C. Koch: Scr. Mater. **49** (2003) 657–662.
5) R.Z. Valiev and Y.T. Zhu: Trans. Mater. Res. Soc. Jpn. **40** (2015) 309–318.
6) F. Nogata and H. Takahashi: Compos. Eng. **5** (1995) 743–751.
7) N. Reznikov, M. Bilton, L. Lari, M.M. Stevens and R. Kroger: Science **360** (2018) eaao2189.
8) M. Koyama, Z. Zhang, M.M. Wang, D. Ponge, D. Raabe, K. Tsuzaki, H. Noguchi and C.C. Tasan: Science **355** (2017) 1055–1057.
9) S.C. Zuo and Y.G. Wei: Acta Mech. Solida Sin. **20** (2007) 198–205.
10) T.H. Fang, W.L. Li, N.R. Tao and K. Lu: Science **331** (2011) 1587.
11) X.L. Wu, M.X. Yang, F.P. Yuan, G.L. Wu, Y.J. Wei, X.X. Huang and Y.T. Zhu: Proc. Nat. Acad. Sci. U.S.A. **112** (2015) 14501–14505.
12) Z.N. Li, P.Q. La, J.Q. Ma, X. Guo, J. Sheng, Y. Shi and X.Y. Zhou: Mater. Lett. **238** (2019) 191–193.
13) Y.M. Wang, M.W. Chen, F.H. Zhou and E. Ma: Nature **419** (2002) 912–915.
14) H.D. Wang, P.Q. La, X.M. Liu, Y.P. Wei and T. Shi: Mater. Sci. Eng. A **582** (2013) 1–7.
15) G.C. Ma, J. Sheng, Q. Meng, M.C. Du, P.Q. La, Y.H. Zheng, Y. Wei, F.Q. Zhan and D. Wu: Integr. Ferroelectr. **217** (2021) 190–197.
16) J. Sheng, P.Q. La, J.Q. Su, J.Q. Ren, J.Q. Ma, Y. Shi, Z.N. Li and J. Wang: Mod. Phys. Lett. B **32** (2018) 1850182.
17) J. Sheng, J.C. Li, P.Q. La, F.A. Wei, Y. Song and K.L. Wang: Sci. Adv. Mater. **9** (2017) 1020–1027.
18) L. Chen, F.P. Yuan, P. Jiang and X.L. Wu: Mater. Sci. Eng. A **551** (2012) 154–159.
19) E. Ma: JOM **58** (2006) 49–53.
20) Z. Wang, D. Yin, W. Zhu and H. Li: Value Eng. **26** (2018) 161–162.
21) S.K. Ghosh, D. Mahata, R. Roychaudhuri and R. Mondal: Bull. Mater. Sci. **35** (2012) 839–846.
22) X.L. Wu and Y.T. Zhu: Mater. Res. Lett. **5** (2017) 527–532.
23) E. Ma and T. Zhu: Mater. Today **20** (2017) 323–331.